# 2001 International Electric Propulsion Conference

IEPC-01-238

## Performance Measurements Using a Sub-Micronewton Resolution Thrust Stand

John K. Ziemer
Jet Propulsion Laboratory
California Institute of Technology

27TH IEPC, October 15-19, 2001
Pasadena, California, USA

# Performance Measurements Using a Sub-Micronewton Resolution Thrust Stand*

John K. Ziemer
Jet Propulsion Laboratory, M/S 125-109
California Institute of Technology
4800 Oak Grove Drive, Pasadena, CA 91109
(818) 393-4582, John.K.Ziemer@jpl.nasa.gov

IEPC-01-238†

**A sub-micronewton level thrust stand is used to evaluate the performance of five different microthrusters. Using a torsional balance design, the JPL microthrust stand ($\mu$TS) is capable of measuring steady-state thrust as low as 1 $\mu$N with sub-micronewton resolution and an impulse as low as 1 $\mu$Ns with sub-micronewton-second resolution. The $\mu$TS can support a test object with a mass as large as 10 kg while supplying multiple diagnostic, power, and propellant lines to the thruster. The thrust or impulse is measured by monitoring the position of the thrust arm and using a calibrated dynamic model that will be presented in this paper. The performances of a vacuum arc thruster (VAT), gas-fed pulsed plasma thruster (GFPPT), indium field emission electric propulsion thruster (In-FEEP), vaporizing liquid microthruster (VLM), and micro-cold gas thruster have been measured using this test stand to validate its accuracy and precision.**

## 1 Introduction

Micropropulsion devices that are designed to produce micronewtons of thrust are being developed in many industrial, government, and academic laboratories around the world [1]. This effort is in response to missions that plan to use microspacecraft or that require extremely precise thrust levels. For example, many upcoming "drag-free" missions such as LISA, STEP, MICROSCOPE, EX5, LIRE, MAXIM, TPF, and Stellar Imager will require various microthrusters that can provide between 0-1000 $\mu$N with precision requirements as small as 0.1 $\mu$N. Until fairly recently, direct measurement of the thrust produced by such devices has not been possible by conventional thrust stands.

Over the last few years, many micronewton and sub-micronewton thrust stands have been developed in parallel at institutions including, among others, BUSEK Co. Inc. [2], US Air Force and USC [3], NASA Goddard and the University of Maryland [4], and ONERA in France [5]. Thrust stands designed to measure the impulses produced by pulsed microthrusters that can also be used to measure steady-state thrust have been built at Princeton University [6], the University of Illinois [7], NASA Glenn [8], and many other institutions. Although each method of impulse or thrust measurement may be slightly different, most microthrust stands have been designed and tested with only one type of thruster in mind.

This paper describes the development and testing of a microthrust stand ($\mu$TS) in the Advanced Propulsion Technology Laboratory at NASA Jet Propulsion Laboratory (JPL). Originally constructed from a torsional pendulum design provided by the Electric Propulsion and Plasma Dynamics Laboratory (EPPDyL) at Princeton University [6], the thrust stand described in this paper has been modified to accept a variety of thruster types and diagnostic packages. The $\mu$TS has been used to measure both thrust and impulse produced by many thrusters currently under

*Copyright ©2001 by California Institute of Technology. Published by the Electric Rocket Propulsion Society with permission.

†Presented at the 27th International Electric Propulsion Conference, Pasadena, CA, 15-19 October, 2001.

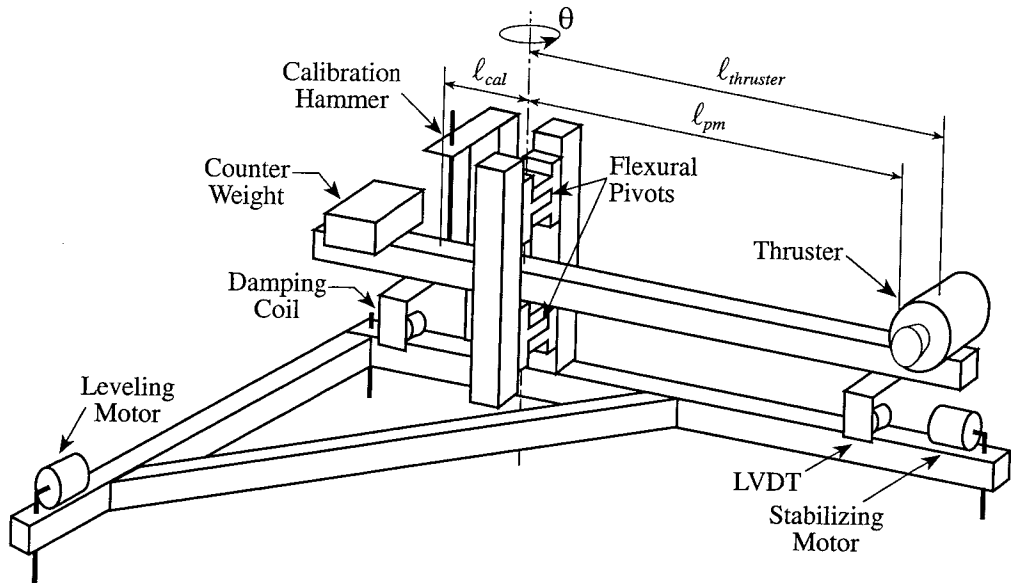


Figure 1: Drawing of the $\mu$TS. Positions of the thruster, LVDT, calibration hammer, and rotational axis are shown by markers.

development. To date, these thrusters include: a vacuum arc thruster (VAT) [9], gas-fed pulsed plasma thruster (GFPPT) [10], indium field emission electric propulsion thruster (In-FEEP) [11], vaporizing liquid microthruster (VLM) [12], and a micro-cold gas thruster developed by Moog, Inc. The goal of this research has been to develop a useful test-bed for the advancement of micropropulsion research and provide a way to evaluate candidate thrusters for some of the missions mentioned above.

This paper is organized as follows: we begin in the first section by deriving a model for torsional pendulum dynamics. This model is developed to the point where the impulse and thrust can be determined from the position history of the thrust arm motion. Next, the performances of various microthrusters are presented with a focus on how the unique capabilities of the JPL microthrust stand were used to provide useful information about each thruster. Finally, in the appendix, a model for how mechanical vibrations are related to thrust stand resolution is presented.

## 2 Torsional Pendulum Dynamics

The $\mu$TS is fundamentally a torsional pendulum. The test mass or thruster is mounted to a horizontal arm which is supported by two flexural pivots as shown in Fig. (1). To reduce the influence of gravity, the thruster is counter-balanced so the center of mass (CG) of the entire thrust arm is close to the pivot axis. As shown in the appendix, this arrangement leads to the highest possible sensitivity. With a small contribution from gravity, the restoring torque is linearly proportional to the displacement angle, $\theta(t)$, and the effective spring constant, $k_{theta}$, created mainly by the stiffness of the pivots and connecting cables.

The dynamics of this type of system have been described many times in other sources and will only be summarized here. The end result is a model of thrust stand motion or angular deflection, as a function of the time-dependent force produced by the thruster, $f(t)$. With the thruster mounted at a fixed distance away from the rotational axis, $\ell_{thruster}$, the sum of torques acting on the pendulum, including friction, $\nu\dot{\theta}$, can be written in this form,

$$\ddot{\theta} + 2\zeta\omega_n\dot{\theta} + \omega_n^2\theta = \frac{f(t)\ell_{thruster}}{I_\theta}, \qquad (1)$$

where $I_\theta$ is the moment of inertia, $\zeta$ is the damping coefficient,

$$\zeta \equiv \frac{\nu}{2}\sqrt{\frac{1}{I_\theta k_\theta}}, \tag{2}$$

and $\omega_n$ is the natural frequency,

$$\omega_n \equiv \sqrt{\frac{k_\theta}{I_\theta}}. \tag{3}$$

Assuming that $\omega$, $\zeta$, and $I_\theta$ are constant and not functions of $\theta$ or $t$, the characteristics of the solutions to Eq. (1) are well understood. First, for simplicity, we will call the position of the thrust arm when all torques are balanced as the "neutral position." With the thrust arm initially at rest and in the neutral position, we will now examine its response to two types of forces: impulsive and constant.

### 2.1 Impulsive Force

Subjected to an impulsive force, $f(t) = I_{bit}\delta(t)$, the solution of Eq. (1) is,

$$\theta(t) = \frac{I_{bit}\,\ell_{thruster}}{I_\theta \omega_n \sqrt{1-\zeta^2}}\, e^{-\zeta\omega_n t}\, \sin\left(\omega_n\sqrt{1-\zeta^2}\, t\right), \tag{4}$$

Calculating the impulse bit requires a measurement of the initial angular velocity, the moment of inertia, and the length between the applied force and the rotational axis,

$$I_{bit} = \frac{\dot{\theta}(0) I_\theta}{\ell_{thruster}}. \tag{5}$$

Note that the spring constant, $k_\theta$, does not enter into the calculation of the impulse bit.

### 2.2 Constant Force

Subjected to a constant thrust force, $f(t) = T$, the solution of Eq. (1) is,

$$\begin{aligned}\theta(t) \;=\; & \frac{T\,\ell_{thruster}}{I_\theta \omega_n^2}\Big[1 - e^{-\zeta\omega_n t}\times \\ & \left(\frac{\zeta}{\sqrt{1-\zeta^2}}\sin\left(\sqrt{1-\zeta^2}\,\omega_n t\right) + \right. \\ & \left.\cos\left(\sqrt{1-\zeta^2}\,\omega_n t\right)\right)\Big].\end{aligned} \tag{6}$$

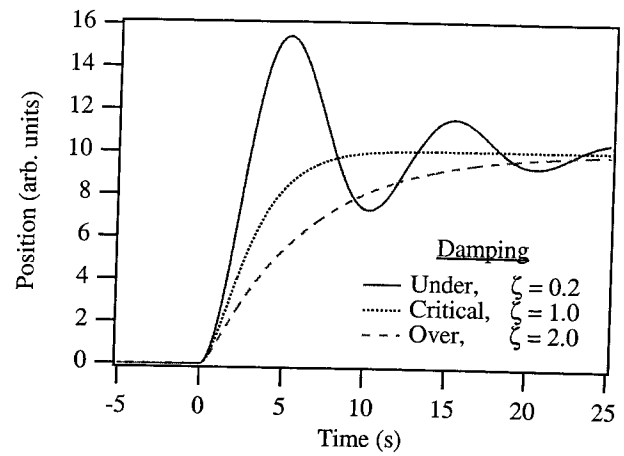


Figure 2: Position as a function of time for under-, critically-, and over-damped solutions to the constant force case, Eq. (6).

Figure 2 shows a plot of Eq. (6) with three different values of $\zeta$ and a natural period of 10 s. Note that if $\zeta = 1$, the thrust arm will reach a new neutral position in the shortest amount of time (roughly one natural period) with no overshoot.

When the thruster has reached a steady-state operating condition, the new neutral position can be found by taking $t \to \infty$ in Eq. (6),

$$\theta(t \to \infty) = \frac{T\,\ell_{thruster}}{I_\theta \omega_n^2} = \frac{T\,\ell_{thruster}}{k_\theta}. \tag{7}$$

Solving for the thrust level,

$$T = \frac{\theta(\infty) k_\theta}{\ell_{thruster}}, \tag{8}$$

which becomes the useful equation for measuring thrust. In reality an infinite time does not actually have to pass before the thrust arm reaches the new position within the limits of the ability to measure $\theta$ accurately. Determining the thrust then comes from calibration data (measurements of $k_\theta$ and $\ell_{thruster}$) and measuring $\theta$ after a number of natural periods. Note that the moment of inertia, $I_\theta$, does not enter into the thrust calculation.

## 3 Measuring Impulse and Thrust

As shown in Eq. (5) and (8), the impulse and thrust can be calculated from real-time measurements of

$\theta(t)$ with the constants $k_\theta$, $I_\theta$, and $\ell_{thruster}$ measured independently as a calibration. These measurements are described below.

### 3.1 Measuring $\theta(t)$

The angular position as a function of time can be measured in many different ways. In the case of small deflections, $\theta < 4°$ for example, the position can be determined within 0.1% by measuring the *linear* displacement, $x(t)$, at some point a distance $\ell_{pm}$ away from the rotational axis, $\theta(t) = x(t)/\ell_{pm}$.

In many cases, the linear displacement can be measured more accurately than the angular displacement, but at the expense of the error associated with measuring another constant, $\ell_{pm}$. Furthermore, any error in measuring $x(t)$ will translate to errors in the impulse or thrust measurement so the position measurement device must be very accurate and precise. Many methods for measuring position or acceleration have been used in other thrust stand designs such as laser interferometry [6], capacitive measurements [4], fiber optics [2], high-resolution accelerometers [5], and others. In our case, we use a Linear Voltage Displacement Transducer (LVDT) that has sub-micron resolution for its simplicity of operation and ease of interpreting the linear voltage output proportional to position.

With a linear position measurement, the impulse bit becomes,

$$I_{bit} = \frac{\dot{x}(0) I_\theta}{\ell_{thruster}\, \ell_{pm}}, \tag{9}$$

and the thrust can be expressed as,

$$T = \frac{x_{final} k_\theta}{\ell_{thruster}\, \ell_{pm}}. \tag{10}$$

Measuring $\dot{x}(0)$ or $x_{final}$ for impulse or thrust calculation, respectively, consists of curve fitting the position history using Eq. (4) or taking the average of the thrust arm position after a few natural periods. In practice, there is also a small amount of background motion or drift that must be subtracted before determining the impulse or thrust. In the case of impulse measurements, a damped sinusoid is also fit to the position history *before* the impulse and the actual measurement is $\Delta\dot{x}(t = 0)$. In the case of thrust measurements, the drift rate is assumed to be constant over the test and is subtracted based on a linear fit of the baseline data before and after thruster operation. Measuring $k_\theta$, $I_\theta$, $\ell_{thruster}$, and $\ell_{pm}$ must be done as a calibration before the thrust or impulse measurement.

### 3.2 Thrust Stand Calibration

The four constants $k_\theta$, $I_\theta$, $\ell_{thruster}$, and $\ell_{pm}$ can be found by supplying a known impulse, $I_{cal}$, at some distance from the pivot axis, $\ell_{cal}$, and monitoring the response of the thrust arm. To derive the relationship between the calibration constants and the position history, first we define a useful quantity called the *effective mass*, $m_{eff}$,

$$m_{eff} \equiv \frac{I_\theta}{\ell_{thruster}\, \ell_{pm}}. \tag{11}$$

The impulse and thrust calculations then follow from Eqs. (9) and (10),

$$I_{bit} = \dot{x}(0)\, m_{eff}, \tag{12}$$

$$T = x_{final}\, m_{eff}\, \omega_n^2. \tag{13}$$

The effective mass can be found from the calibration impulse and a measurement of $\ell_{cal}/\ell_{thruster}$,

$$m_{eff} = \frac{I_{cal}}{\dot{x}(0)} \frac{\ell_{cal}}{\ell_{thruster}}, \tag{14}$$

In this case, the initial velocity, $\dot{x}(0)$, and the natural frequency can be found from curve fitting a damped sinusoid to the position history obtained during the calibration (as long as $\zeta < 1$). Note that $\ell_{pm}$ does not need to be measured unless a calculation of the moment of inertia is desired. Furthermore, if the calibration impulse is delivered at the same position as the force produced by the thruster, then no lengths need to be measured at all.

With the $\mu$TS, the known impulse is supplied to the thrust arm by a piezoelectric force transducer mounted at the end of a rod called the "calibration hammer," as shown in Fig. (1). The mounting rod is cocked at an angle by an electromagnet that is switched off to release the hammer. Upon impact,

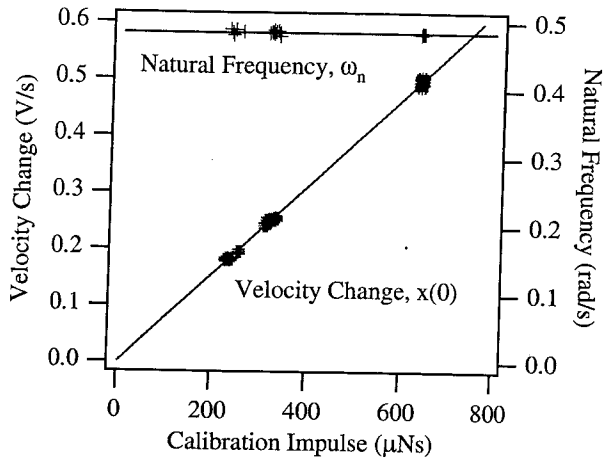


Figure 3: Velocity change and natural frequency as a function of the delivered calibration impulse. The graph shows the results of 25 trials at various cocking angles.

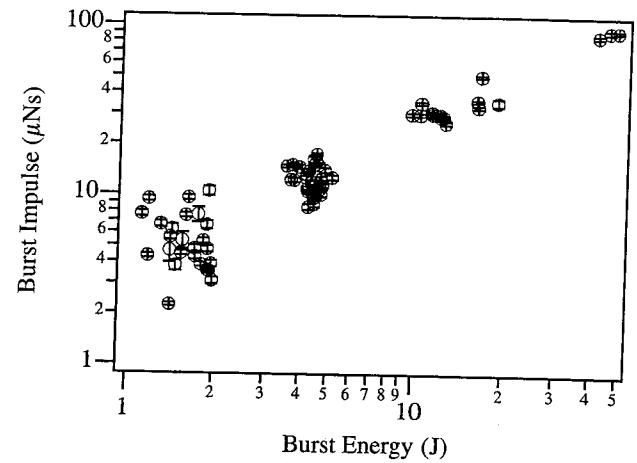


Figure 4: Impulse produced by a titanium cathode Vacuum Arc Thruster (VAT) as a function of the energy stored before the burst. Each point represents an impulse measurement from a burst of 25 pulses. The goal of this research was to determine the performance and repeatability of the VAT.

the transducer outputs a voltage proportional to the instantaneous force which can then be integrated to determine the calibration impulse. The impulse magnitude can be changed by changing the cocking angle of the electromagnet. Figure 3 shows a range of calibration impulses used to find the effective mass and the natural frequency. Usually both quantities can be found with a standard deviation less than 1% of the measured quantity over at least 20 trials, including error from position measurement and force transducer calibration. Finally, note that in our case the "position" measurement is really a voltage measurement, yet this does not change the method of calibration or any force calculation. The effective mass simply has the units of [kg-m/V], and the position measurement is kept in terms of volts instead of meters. The conversion between voltage and position is required only if a real value of mass or the moment of inertia is desired.

# 4 Performance Measurements

The performance of five different thrusters has been measured using the $\mu$TS including a vacuum arc thruster (VAT), gas-fed pulsed plasma thruster (GFPPT), indium field emission electric propulsion thruster (In-FEEP), vaporizing liquid microthruster (VLM), and micro-cold gas thruster. In each of the following sections a brief description of the technology will be followed by an outline of the challenges involved with the measurements and what was accomplished in each case. The purpose of this section is *not* to discuss the technology development of each microthruster in detail (full descriptions can be found in the literature [9, 10, 11, 12]) but to present the capabilities of the JPL microthrust stand as a diagnostic tool.

## 4.1 VAT Impulse Measurements

A vacuum arc thruster (VAT) operates in a pulsed mode by ablating a small amount of cathode material (in our case titanium) with an inductively driven arc [9]. Normally, impulse bits are so small that burst of pulses are grouped together with the energy for all the pulses stored in a single capacitor before the burst. The challenge in measuring the impulse produced by a VAT is simply the small magnitude, as low as 2 $\mu$Ns.

In this test, the burst capacitor was charged to a fixed voltage and the thruster was commanded to fire 25 times in one burst. As shown in Fig. (4), over 100 impulse measurements at various voltage levels

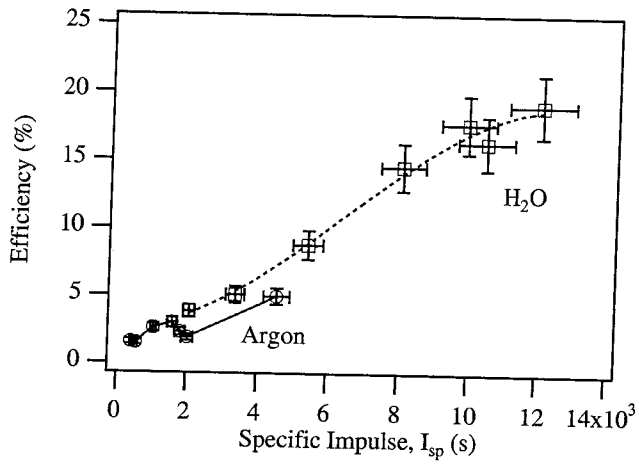


Figure 5: Thrust efficiency as a function of specific impulse for PT8, a gas-fed pulsed plasma thruster (GFPPT). The goal of this research was to determine the difference in performance between argon and water vapor propellants.

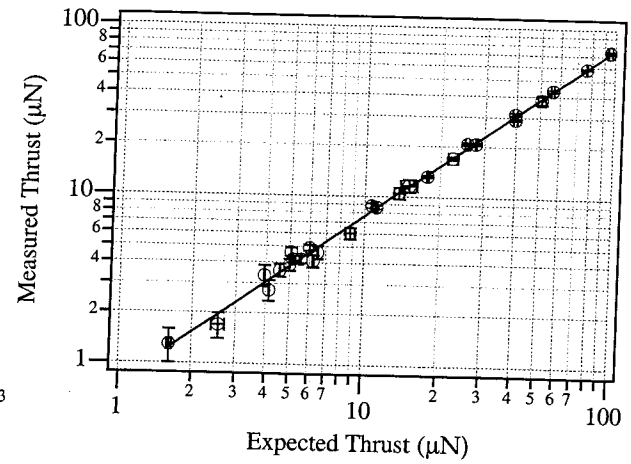


Figure 6: Measured thrust as a function of expected thrust (based on Eq. (15)) for an indium field emission electric propulsion thruster (InFEEP). The goal of this research was to measure the range of thrust the InFEEP can produce with high precision.

were conducted in less than two hours. The purpose of these measurements was to examine the impulse-to-energy ratio and the repeatability of the impulse produced by the VAT. From the results of this test, the $\mu$TS demonstrated an ability to measure impulse with sub-micronewton-second precision and to provide a large data set for statistical measurements.

## 4.2 GFPPT Performance Measurements

A gas-fed pulsed plasma thruster (GFPPT) uses a high-current arc discharge to accelerate plasma through a self-field Lorentz force [10]. GFPPTs can use a wide variety of gaseous propellants including noble gases, hydrocarbons, water vapor, etc. The challenge in calculating the performance of a GFPPT is the simultaneous nature of all of the required measurements: impulse, energy, mass bit, specific impulse, and efficiency. For the GFPPT to operate correctly, the capacitor bank is charged and the valve is opened just before the discharge, creating small disturbances that could be interpreted as an additional impulse.

In this test, both argon and water vapor were used as propellants with the same GFPPT, PT8. As shown in Fig. (5), the $\mu$TS was used to show that performance is higher with water vapor at the same specific impulse. In all cases, the background disturbances were measured and subtracted for each pulse. In addition, each data point is actually an average of one operating condition repeated at least 20 times. Using this test, the $\mu$TS once again demonstrated the ability to produce a large amount of data in a relatively short amount of time. It was also shown that a variety of propellants can be used with the stand, and that background disturbances as small as 1 $\mu$Ns can be successfully measured and subtracted from the real impulse measurements.

## 4.3 InFEEP Thrust Measurements

An indium field emission electric propulsion (InFEEP) thruster uses a high voltage to accelerate liquid-metal ions to a high velocity [11]. A 1-2 W heater is used to melt the metal propellant (in this case indium), and between 5-10 kV is used to extract and accelerate the ions. The challenge in measuring the thrust produced by an InFEEP is the small magnitude of the thrust, between 1-100 $\mu$N, and the high voltage cable interaction with the thrust stand facility itself.

In this test, measurements were made over a wide range of discharge current and voltage values to examine the dynamic thrust range of the InFEEP

thruster. As shown in Fig. (6), the $\mu$TS was used to measure thrust with unprecedented precision in the full range of the InFEEP operation, 1-100 $\mu$N. To solve the problem of the high voltage interaction with the facility, a DC-DC converter was used to produce the high voltage very close to the thruster (on the thrust stand itself), so that only relatively low voltage cabling was required. Using this technique, the thrust produced by the InFEEP was compared to the expected thrust based on a model of the discharge current and voltage,

$$T = I\sqrt{V}\sqrt{\frac{2m_w}{e}}, \tag{15}$$

where $I$ is the discharge current, $V$ is the discharge voltage, and $m_w$ is the propellant molecular weight. From a linear fit of the data, the measured thrust was close to 80% of the expected thrust, agreeing with recent measurements made at ONERA [5].

As shown in Fig. (7), the precision of the $\mu$TS was evaluated by setting the InFEEP thruster to produce approximately 1 $\mu$N of thrust. To initiate the discharge, a higher voltage was used at first and gradually reduced to the correct value. Unfiltered, the standard deviation on an average of the thrust measurement over a few natural periods was approximately $\pm 0.3$ $\mu$N. Using a 0.1 Hz low pass filter, the standard deviation was even less, closer to $\pm 0.1$ $\mu$N. This cut-off frequency corresponds to the natural frequency of the thrust stand. Higher frequency measurements of thrust disturbances were not possible with the $\mu$TS in this configuration.

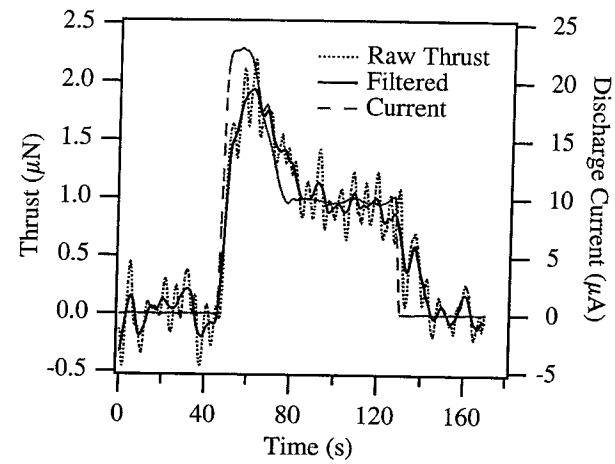


Figure 7: Measured thrust for the InFEEP thruster operating at very low discharge current. Traces of the raw and filtered (0.1 Hz low pass filter) thrust data along with discharge current. The goal of this research was to examine the precision and frequency response of the microthrust stand.

## 4.4 VLM Thrust Measurements

The vaporizing liquid microthruster (VLM) is a MEMS-based technology that heats and vaporizes water propellant to produce thrust [12]. The challenge in measuring the thrust produced by the VLM is due to the complex nature of the thrust stand setup. Ten feed lines and cables were required for heater power, valve control, pressure and temperature monitoring. The water was stored on board the thrust stand and pressurized using yet another feed line. Mounting the cables to provide the necessary diagnostics while maintaining thrust stand resolution was difficult.

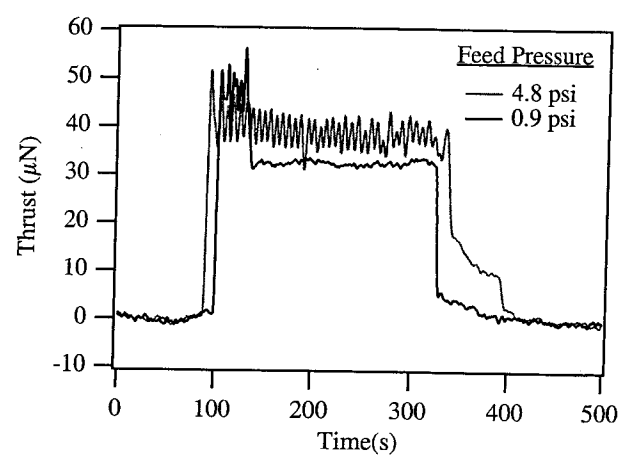


Figure 8: Measured thrust for two different feed pressures of the vaporizing liquid microthruster (VLM). The goal of this research was to find the proper feed pressure for stable operation of the VLM.

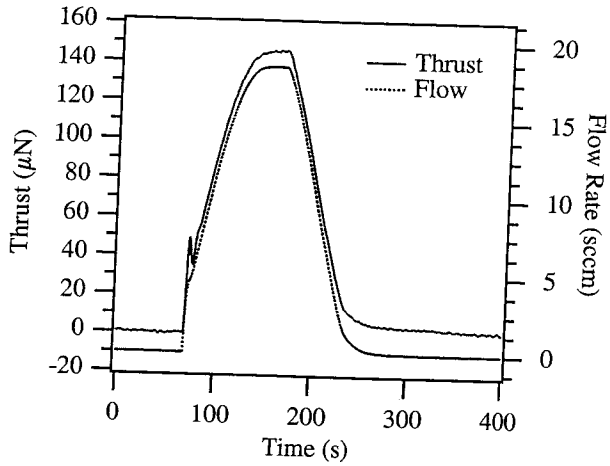


Figure 9: Measured thrust and flow rate for the Moog micro-cold gas thruster. The flow rate was varied by throttling a valve over the span of the test. The goal of this research was to measure the thrust and specific impulse over a wide range of operating conditions.

The $\mu$TS was used to examine the stability of the thrust produced at various feed pressures and corresponding water flow rates. If the water flow rate is too high, only a portion of the water is vaporized before exiting the nozzle and periodic bursts of gas make the thrust unstable. At lower feed pressures, the water flow rate is small enough so that all the water is vaporized, and the VLM thrust output is stable. These two conditions were observed using the $\mu$TS and are shown in Fig. (8).

### 4.5 Micro-Cold Gas Thruster Specific Impulse Measurements

The micro-cold gas thruster under development at Moog, Inc. is designed to provide a wide range of thrust from 1-1000 $\mu$N. A very fine control valve controls both the flow and the thrust for this micropropulsion device. The challenge in measuring the specific impulse for this thruster is the wide range of operating conditions that need to be evaluated.

One way of measuring thrust over a large range of flow rates is to sweep the valve position over part of its full stroke. The microthrust stand was set up with the highest frequency response possible so that the sweep could take place in a reasonably short time. As shown in Fig. (9), the $\mu$TS response followed the flow rate extremely well.

## 5 Summary

The JPL microthrust stand has been used effectively to measure thrust and impulse from a variety of micropropulsion devices. The resolution of the $\mu$TS has been characterized experimentally as $<1$ $\mu$N for steady-state thrust measurements and $<1$ $\mu$Ns for impulse measurements. Although high frequency ($>1$ Hz) response cannot be studied with the $\mu$TS, it has proven quite useful and versatile as a diagnostic tool in developing a number of micropropulsion devices.

## Acknowledgements

The author wishes to acknowledge the people that have helped in developing the $\mu$TS by supplying devices to test: Jochen Schein from Alameda Applied Sciences Corp., Jonah Jacob from Science Research Laboratory, Inc., Martin Tajmar from Austrian Research Centers Seibersdorf, Juergen Mueller from the Jet Propulsion Laboratory, and Richard Meinhold from Moog, Inc..

The research described in this paper was carried out at the Jet Propulsion Laboratory, California Institute of Technology, under a contract with the National Aeronautics and Space Administration.

## A APPENDIX: Influence of Gravity and External Vibrations

Until now our analysis has not included the effects of gravity or of having a rotational plane that is not exactly horizontal. Including gravity makes the problem inherently non-linear except in the limit of a small deflection angle. For that reason and for the practical reason that we are measuring a linear displacement, we will constrain the thrust stand motion to small angles. Still, the gravitational torque caused by an off-axis center of mass and/or a tilted rotational axis can be significant and will shift the neutral position of the thrust arm. In practice it is very difficult to get either the center of mass exactly on the rotational

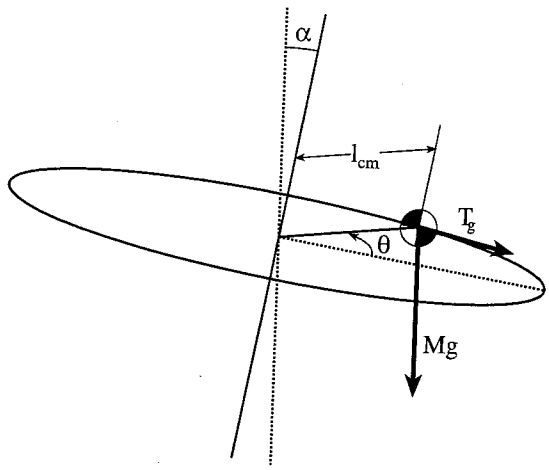


Figure 10: Schematic of a torsional pendulum with center of mass located a distance $\ell_{cm}$ away from the rotational axis, and a rotational axis that is at an angle $\alpha$ from vertical (shown as a dotted line). The thrust arm is shown deflected from the neutral position (also shown as a dotted line) by an angle $\theta$.

axis or to have a rotational axis that is exactly vertical due to misalignment or mechanical vibrations. This section of the paper will examine the effects of the gravitational torques in terms of how changes in the angle of the rotational plane effect the spring constant and neutral position.

### A.1 Effect of the Stability Angle, $\alpha$

The stability angle, $\alpha$, is defined schematically in Fig. (10) and can be seen visibly as a tilt in the thrust arm from a front-on view. For $\alpha \neq 0$, the rotational axis is tilted in a plane that also contains the neutral position of the thrust arm (where the spring torque and gravity torque are both zero) defined previously in Section 2. If the thrust arm is deflected by an angle $\theta$, the torque caused by gravity, $T_g$, is,

$$T_g = \ell_{cm} M g \sin\alpha \left(1 - \cos\theta\right). \tag{16}$$

Note that the gravitational torque is positive as long as $\alpha$ is positive and only non-zero when $\theta$ is non-zero (i.e. the neutral position remains fixed). That is, the torque caused by gravity will always augment the torque caused by the spring as long as $\alpha$ is positive, making the system stable. If $\alpha$ is less than zero, as it becomes more and more negative the gravitational torque will fight against the spring torque and the system will eventually become unstable. For small values of $\theta$, the criteria for a stable system is,

$$\alpha > \frac{-2k_\theta}{\ell_{cm} M g \theta}. \tag{17}$$

We should also note that the gravitational torque is *not* linear in $\theta$ like the spring torque. This can cause a problem for thrust measurements if $\theta$ is large and the gravitational torque is of the same magnitude as the spring torque. Since for small deflection angles this only has the effect of changing the effective spring constant in a linear fashion, we can set a *maximum* criteria on the size of $\alpha$ to minimize the gravitational influence. When combined with the minimum criteria in Eq. (17), we obtain the following limit for stable, linear, and accurate thrust measurement,

$$|\alpha| < \frac{k_\theta}{\ell_{cm} M g \theta_{max}}. \tag{18}$$

Three interesting ways of meeting this requirement are to have $\alpha, M$, or $\ell_{cm}$ close to zero in value. Again, in practice for any of the parameters, that can be difficult to achieve. In fact, we will see in the next section that having a large mass is beneficial in terms of vibrational noise while, at the same time, we must insure that $\alpha$ (and thus the effective spring constant including gravity) remains the same between calibration and thrust measurement. With that in mind, having the smallest value of $\ell_{cm}$ is obviously beneficial.

### A.2 Effect of the Position Angle, $\beta$

As shown in Fig. (11), $\beta$ is the angle of the rotation axis orthogonal to $\alpha$. Changing $\beta$ results in a large shift of the gravity neutral position. For example, if $\alpha = 0$, then even the smallest change in $\beta$ results in the gravity neutral position shifting by 90° and the final rest position (where the gravitational torque and spring torque are equal) shifting by a large amount. In an analogy to the effect of changing $\alpha$, the magnitude of the influence of gravity depends on the magnitude of $\beta$,

$$\begin{aligned} T_g &= \ell_{cm} M g \sin\beta \left(1 - \sin\theta\right) \\ &= \ell_{cm} M g \sin\beta \left(1 - \cos\left(\theta - \frac{\pi}{2}\right)\right), \end{aligned} \tag{19}$$

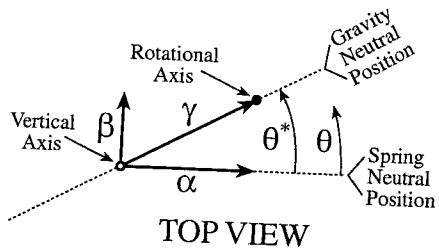


Figure 11: The angles $\alpha, \beta$, and $\gamma$ are defined in terms of the spring neutral position, the rotational axis, and the gravity neutral position (at an angle $\theta^*$).

with $\alpha = 0$.

As shown in Eq. (19), changing $\beta$ does not create any instability, but it does result in a new neutral position where the gravitational and spring torques are equal,

$$\theta_{neut} \approx \frac{\ell_{cm} M g \beta}{k_\theta}, \tag{20}$$

where, again, a small angle assumption has been made for $\theta$ and $\beta$. Notice that the new neutral position is approximately linearly dependent on $\beta$. Since, in many cases, the position must be measured accurately within microns, small and permanent changes in $\beta$ can be important. To reduce their influence, once again we see that having the center of mass on the rotational axis ($\ell_{cm} \approx 0$) is beneficial.

## A.3 Effect of Changing Both $\alpha$ and $\beta$

Together, $\alpha$ and $\beta$ explicitly determine the orientation of the rotational plane. Changing both the stability angle, $\alpha$, and the position angle, $\beta$, has the effect of changing the degree of influence of gravity and shifting the neutral position. Using the diagram in Fig. (11) as guide, we define a new angle $\gamma$ with the relation,

$$sin^2\gamma = sin^2\alpha + sin^2\beta. \tag{21}$$

The new gravitational neutral position is in the plane between the vertical axis and the rotational axis at an angle $\theta^*$ from the spring neutral position. The gravitational torque is then,

$$\begin{aligned} T_g &= \ell_{cm} M g \sin\gamma \left(1 - \cos\left(\theta - \theta^*\right)\right) \\ &= \ell_{cm} M g \left(\sin\gamma - \cos\theta \ \sin\alpha - \sin\theta \ \sin\beta\right), \end{aligned} \tag{22}$$

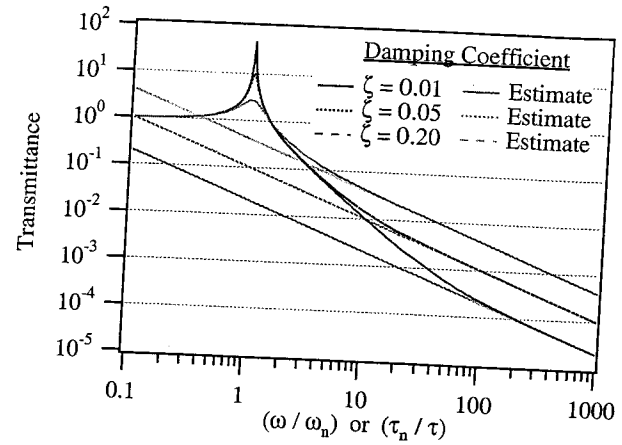


Figure 12: Transmittance as a function of the external vibration frequency, $\omega_{ex}$, and the natural frequency of the thrust arm, $\omega_n$. Estimations based on Eq. (26) are included as slightly lighter lines.

where,

$$\cos\theta^* = \frac{\sin\alpha}{\sin\gamma} \tag{23}$$

$$\sin\theta^* = \frac{\sin\beta}{\sin\gamma}. \tag{24}$$

Note that if $\beta = 0$ or $\alpha = 0$ the gravitational torque returns to the form in Eq. (16) and Eq. (19), respectively. Similarly, Eq. (20) becomes,

$$\theta_{neut} \approx \frac{\ell_{cm} M g \gamma}{k_\theta}. \tag{25}$$

Ultimately, the best way to reduce the influence of the gravitational torques is to have the smallest $\ell_{cm}$ possible.

## A.4 Effects of External Vibration

External vibrations essentially have the effect of changing $\alpha$ and $\beta$ as the base that supports the thrust stand oscillates. Although the change in the angles may be small, as shown in Eq. (25), small changes, especially in the position angle, $\beta$, can result in significant motion of the arm. The maximum resolution of the thrust stand is dictated by the amount of background vibrational noise in the measurement of position.

Another important factor in determining the extent of the vibration effect is the ratio of the vibration

frequency, $\omega_{ex}$, to the natural frequency of the thrust stand, $\omega_n$. The transmission, $\mathcal{T}$, of the vibration is related to,

$$\mathcal{T} = \sqrt{\frac{1+\left(2\zeta\frac{\omega_{ex}}{\omega_n}\right)^2}{\left(1-\left(\frac{\omega_{ex}}{\omega_n}\right)^2\right)^2+\left(2\zeta\frac{\omega_{ex}}{\omega_n}\right)^2}} \approx 2\zeta\frac{\omega_n}{\omega_{ex}}. \tag{26}$$

A graph of the transmittance and the estimated transmittance as a function of $\omega_{ex}/\omega_n$ is shown in Fig. (12).

We can now estimate the maximum resolution of the thrust stand starting with Eq. (13),

$$\Delta T = \Delta x \; m_{eff} \; \omega_n^2. \tag{27}$$

The change in the position, $\Delta x$, is determined by the change in $\gamma$ from Eq. (25). The change in $\gamma$ is, in turn, proportional to the transmission of vibration from the base to the thrust stand, Eq. (26). Putting these relations together and simplifying yields,

$$\begin{aligned} \Delta T &= Mg\left(\frac{\ell_{cm}}{\ell_{thruster}}\right)\mathcal{T}\,\Delta x_{base} \qquad (28)\\ &\approx 2Mg\,\zeta\left(\frac{\ell_{cm}}{\ell_{thruster}}\right)\left(\frac{\omega_n}{\omega_{ex}}\right)\Delta x_{base}. \end{aligned}$$

Equation (28) shows that having a small total mass, damping coefficient, $\ell_{cm}$, and natural frequency along with a large thrust arm length and vibrational frequency leads to high thrust resolution. Having a small vibrational displacement ($\Delta x_{base}$) to begin with is beneficial, however, this may not be possible due to the nature of the test facility.

It is interesting to note that the spring constant of the arm does not directly enter into the resolution equation except through the natural frequency and the resolution of the position measurement device. This is true because, for example, although a stiffer spring will lead to less displacement for the same amount of thrust, it will not be as susceptible to vibration. Still, a lighter spring and a large moment of inertia will lead to a large natural period which is desirable. Overall, a thrust stand with a small amount of mass that is positioned far away from the rotational axis will have the best resolution. In fact, if the thruster is mounted far away from the rotational axis with the mass distributed so that the moment of inertia is large *and* the center of mass is on the rotational axis ($\ell_{cm} \approx 0$), then the resolution is maximized.

## References


[1] J. Mueller. *Thruster Options for Microspacecraft: A Review an Evaluation of State-of-the-Art and Emerging Technologies*, volume 187 of *AIAA Progress in Astronautics and Aeronautics*, chapter 3. AIAA, 2000.

[2] M. Gamero-Castano and V. Hruby. A Torsional Balance that Resolves Sub-Micro-Newton Forces. In $27^{th}$ *International Electric Propulsion Conference*, Pasadena, California, October 15-19 2001. IEPC 01-235.

[3] A.D. Ketsdever, A. Jamison, and E.P. Muntz. Accurate Measurement of Sub-Micro-Newton Thrust for Micropropulsion System Performance Characterization. In $27^{th}$ *International Electric Propulsion Conference*, Pasadena, California, October 15-19 2001. IEPC 01-236.

[4] T.N. McKnight, M. Lewis, and A. Baz. Magnetic Suspension Micro-Newton Thrust Stand. In $27^{th}$ *International Electric Propulsion Conference*, Pasadena, California, October 15-19 2001. IEPC 01-237.

[5] J. Bonnet, J.P. Marque, and M. Ory. Development of a Thrust Balance in the microNewton Range. In $3^{rd}$ *International Conference on Spacecraft Propulsion*, 2000.

[6] E.A. Cubbin, J.K. Ziemer, E.Y. Choueiri, and R.G. Jahn. Laser Interferometric Measurements of Impulsive Thrust. *Review of Scientific Instruments*, 68(6):2339–2346, 1997.

[7] M.J. Wilson, S.S. Bushman, and R.L. Burton. A Compact Thrust Stand for Pulsed Plasma Thrusters. In $25^{th}$ *International Electric Propulsion Conference*, Cleveland, Ohio, August 24-28 1997. IEPC 97-122.

[8] T.W. Haag. Thrust stand for pulsed plasma thrusters. *REVIEW OF SCIENTIFIC INSTRUMENTS*, 68(5):2060–2067, 1997.

[9] J. Schein, J.K. Ziemer, N. Qi, R. Binder, J.E. Polk, and M. Krishnan. Low Mass Vacuum Arc Thruster System for Station Keeping Missions. In $27^{th}$ *International Electric Propulsion Conference*, Pasadena, California, October 15-19 2001. IEPC 01-238.

[10] J. Blandino, D. Birx, J.K. Ziemer, and E.Y. Choueiri. Performance and Erosion Measurements of the PT8 Gas-Fed Pulsed Plasma Thruster. Technical Report EPPDyL-JPL99b, NASA Jet Propulsion Laboratory, August 1999.

[11] A. Genovese, M. Tajmar, W. Steiger, and F. Rdenauer. Indium FEEP Endurance Test: Preliminary Results. In $27^{th}$ *International Electric Propulsion Conference*, Pasadena, California, October 15-19 2001. IEPC 01-289.

[12] J. Mueller, I. Chakraborty, D. Bame, and W. Tang. *Vaporizing Liquid Micro-Thruster Concept: Preliminary Results of Initial Feasibility Studies*, volume 187 of *AIAA Progress in Astronautics and Aeronautics*, chapter 8. AIAA, 2000.